A Morphological Study of Energetic Materials: Analysis of Micro-computed Tomography Images to Generate Representative Microstructures

Élodie Kaeshammer, Petr Dokládal, François Willot, B. Erzar, Steve Belon, Lionel Borne

A MORPHOLOGICAL STUDY OF ENERGETIC MATERIALS : ANALYSIS OF MICRO-COMPUTED TOMOGRAPHY IMAGES TO GENERATE REPRESENTATIVE MICROSTRUCTURES

E. Kaeshammer[1,2,3], P. Dokladal[1], F. Willot[1], B. Erzar[2], S. Belon[2], L. Borne[3]

[1] *CMM (Center of Mathematical Morphology), 35 rue St-Honoré, 77300 Fontainebleau, France ;*
[2] *CEA, DAM, CEA-Gramat, 46500 Gramat, France ;*
[3] *ISL (french-german research Institute of Saint-Louis), PO Box 70034-F68301 Saint-Louis Cedex France*

ABSTRACT

In previous work, impact experiments were performed at ISL on three energetic materials composed of 70 % in weight of RDX particles embedded in a wax matrix. These materials differ by the microstructural properties of the explosive particles. The experimental results reveal that the detonation thresholds, and so the sensitivity to shock, are different for each sample. To better understand these results, we characterize the microstructural properties of these compositions and generate virtual microstructures representative of the real microstructures.

First, the microstructures of the three materials are imaged with micro-computed tomography (μCT). The 3D μCT volumes are filtered and segmented. Image processing results are crosschecked with experimental analyses conducted at ISL (weight fraction, particles diameter distribution and particles bulk density distribution) to ensure the reliability of the segmentations. Virtual microstructures of each material are generated with real grains of RDX extracted from the segmented volumes. The virtual microstructures are built to be consistent with the μCT segmented volumes. The morphological granulometry and the spatial covariance of both real and virtual microstructures are compared to verify that the numerical materials are representative of the real materials.

INTRODUCTION

The sensitivity to shock is an important factor in the safety of energetic compositions. A good knowledge of the detonation threshold under impact is necessary for a controlled initiation (choice of the adapted detonators) but also to avoid accidental initiation (for instance a bullet impact). The hot spot theory is commonly used to describe the initiation of energetic materials after an impact [1]. Shock waves interact with the heterogeneities of the material causing elevations of pressure and temperature. In these zones, called hot spots, the temperature can exceed the reactivity threshold. The chemical reaction starts locally. The growth and coalescence of hot spots can lead to the full detonation of the material.

The mechanisms identified in the formation of hot spots are pore collapses [2], shock reflections [3], plastic deformations, friction between grains or fracture of grains [4]. The mechanisms which lead to the formation of hot spots are still not well understood but are strongly dependent on the microstructure.

Several experiments revealed the influence of microstructural parameters on the sensitivity to shock of energetic materials. Some experiments demonstrated the role of the size [5] and the shape of the explosives particles. The influence of the intra-granular defects (porosities and inclusions in the grain of explosive) [6, 7, 8] and extra-granular defects [9] were also investigated.

The long term objective of this work is to quantify the influence of different microstructural parameters on the shock sensitivity (with a focus on the shape of the explosive grains and the intra-granular defects). To do so, we work on three specific materials provided by the ISL. They are composed of 70 % (in weight) of RDX particles embedded in a wax matrix. The microstructures differ as each material is made with a different type of RDX. The first material is made of commercial RS-RDX from Eurenco. This material contains a large number of twinned particles and numerous intra-granular defects (voids and inclusions). The second material is made of raw VI-RDX. Raw VI-RDX grains are obtained after a recrystallization of RS-RDX grains. The recrystallization process reduces the number of intra-granular defects but the

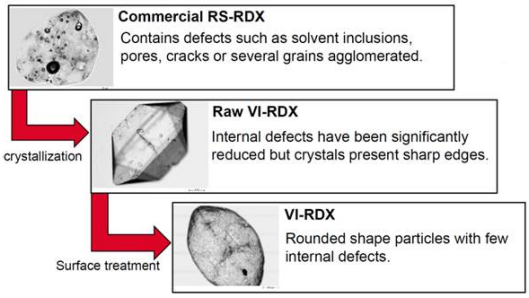

Figure 1: Formulation steps of the VI-RDX

crystals of RDX have now sharp edges. Then a surface treatment process is applied to raw VI-RDX particles to smooth their sharp edges. The resulting VI-RDX particles are patented by ISL. The third material is composed of VI-RDX.

In previous work, impact experiments were performed at the ISL to determine the sustained low pressure shock sensitivity of the three materials. Even if the composition is the same, the detonation thresholds are different: the RS-RDX/Wax and raw VI-RDX/Wax materials detonate for pressure around 6.2 GPa, the VI-RDX/Wax material for a pressure around 7.2 GPa. The RS-RDX and raw VI-RDX based material react for the same pressure despite important microstructural differences. It is supposedly due to two competing microstructural factors: the angular shape and the reduced number of intra-granular defects of the raw VI-RDX grains.

Real materials used in experimental studies are complex as we can find a large number of parameters to describe the microstructures: shape and size of grains, number of intra and extra-granular defects, spatial distribution of the grains, average distance between the grains ... Moreover, some microstructural parameters are correlated (for instance the size of the grain and the number of intra-granular defects). To better understand the influence of some microstructural parameters, we work with virtual materials. With numerical materials, we have a finer control on the microstructure than with real materials. These microstructures must be representative of the real one. To do so, we use real grains extracted from micro-computed tomography images to build virtual geometries.

This paper presents the methodology to build virtual microstructures based on μCT images. The objective is to verify if we are able to reach the correct volume fraction and to reproduce the size distribution of RDX grains. In the first section, a brief description of the micro-computed tomography is given followed by the presentation of the segmented microstructures. The second section introduces the method to create the virtual models. The last section is dedicated to their validation with a comparison of the granulometry and the spatial covariance between the virtual microstructures and the μCT segmented microstructures.

SEGMENTATION OF MICRO-COMPUTED TOMOGRAPHY VOLUMES

We use micro-computed tomography (μCT) to accede to the microstructure of the three materials. This non-destructive technique allows one to visualize in 3D the internal microstructure of a material. Cylindrical samples of 10 mm height and 5mm radius are imaged at the CEA Gramat with a Skyscan 1172 microtomograph. The resolution of acquisition for the materials with RS-RDX and raw VI-RDX grains is 3.67 µm/voxel and 3.54 µm/voxel for the material with VI-RDX grains. Slices extracted from segmented volumes are presented on Fig. 2. The grains appear in dark grey and the wax binder in light gray. The white large spots inside the grains of RDX are intra-granular porosities or solvent inclusions. There are more of them in the RS-RDX than in the VI-RDX particles. In the RS-RDX based material, we also notice agglomerations of grains (highlighted in red on the Fig. 2a) which are twinned grains. The presence of these twinned grains complicates the process of segmentation.

We use the SAMG software, developped at the CMM, to process the 3D images [10]. The image processing is divided into two main parts : the filtering and the segmentation. The step of filtering is necessary to remove the noise. A recursive bilateral filter [11] implemented in SAMG is used. The parameters of the filter are automatically determined with two analyses on the 3D images. The spatial

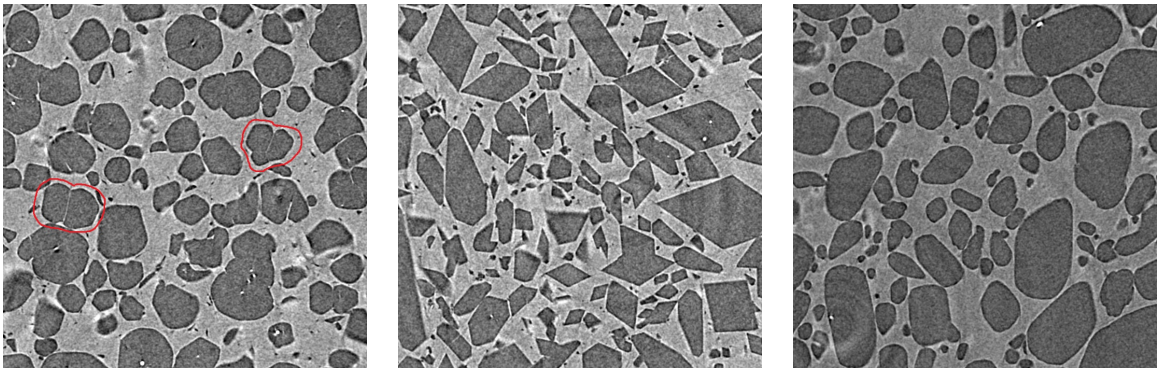

(a) RS-RDX / Wax (b) Raw VI-RDX / Wax (c) VI-RDX / Wax

Figure 2: 600×600 voxels sections extracted from μCT volumes for the three samples. Examples of RS-RDX twinned particles are highlighted on (a).

standard deviation is calculated based on the results of the spatial covariance. The different classes (or phases) in the material are determined by analysing the intensities of the images. The definition of the classes is used to determine the intensity standard deviation parameter of the filter. For the RDX/Wax materials, 2 phases are detected : the RDX grains and the wax binder. The segmentation aims to distinguish the wax binder from the RDX grains but also to individualize each grain of RDX. The segmentation is performed with the watershed algorithm [12]. This algorithm works similarly to a flood of regions. The image is considered as a relief map. The height of each pixel is determined by its intensity: the grains of RDX are dark and thus appear like valleys, the binder is light and thus appears like mountains. Markers are defined as the lowest points of the valley by computing the maximum of the euclidean distance map between the binder and the grains. The relief is flooded from the markers. A virtual frontier is placed when the water flood the neighbouring valley. The barriers are the frontiers of the grains. The watershed algorithm provides a coarse segmentation where the RDX grains are over-segmented (several labels for one grain). A step of over-segmentation correction based on a geometric criterion is used to merge the labels in the over-segmented grains. The geometric criterion quantifies the constriction between two labels: an important constriction means the presence of two touching grains. In this case both labels are kept [13]. A final step of manual correction is performed to correct the remaining segmentation errors. Ten minutes (for the VI-RDX/Wax) to 5 hours (correction of the twinned grains in RS-RDX based material) are necessary to obtain the final segmentation.

One volume of around 1000^3 voxels is segmented for each material. The μCT volume and the corresponding segmented volumes are presented on the Figure 3. The properties of the segmented volumes are summarized in Table 1. Finally, each labelled grain is extracted to constitute a library of grains. The grains cut by the borders of the volume are not considered. But the probability for large grains to be on the border of the volume is more important than for a small particle. Consequently, the diameter distribution of the extracted grains is biased. To correct this bias, we apply the Miles-Lantuejoul correction [14, 15]. This correction consists in assigning to each grain a probability for its bounding box to be fully enclosed in the volume.

To ensure the reliability of the segmentation, segmentation analysis results are crosschecked with experimental data. ISL provides three information that we can compare :

- a theoritical RDX volume fraction of 56 %,
- an experimental distribution of diameter (obtained with Static Light Scattering),
- a cumulative bulk density distribution (obtained with the patented ISL flotation method [16]).

During the segmentation process, a certain amount of RDX is lost between the filtered volume and the segmented volume: very small particles and a few voxels on the boundaries of the grains. The final volume fraction is around 0.54 for the three samples. The computed diameters and bulk densities distributions are consistent with the experimental measures from ISL. The segmented volumes are considered reliable and are exploited to create the library of grains.

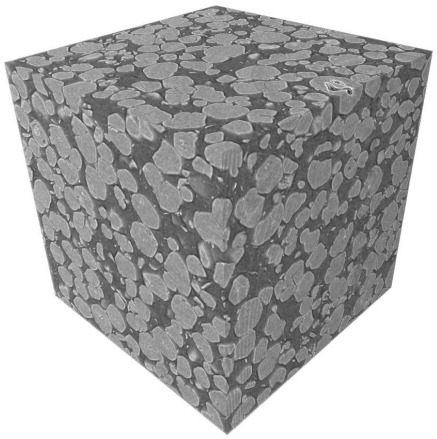

(a) μCT RS-RDX/Wax

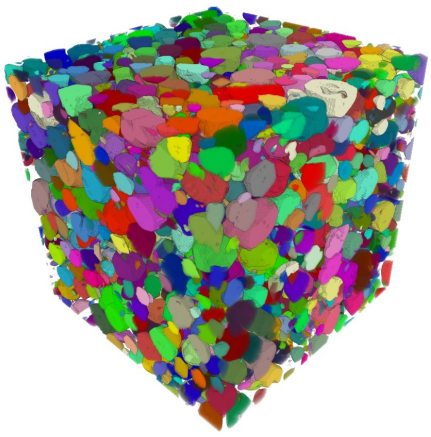

(b) segmented RS-RDX/Wax

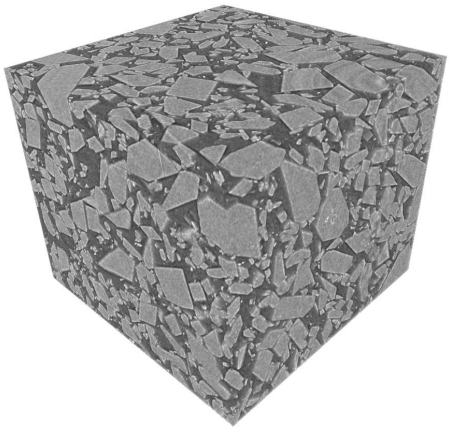

(c) μCT raw VI-RDX/Wax

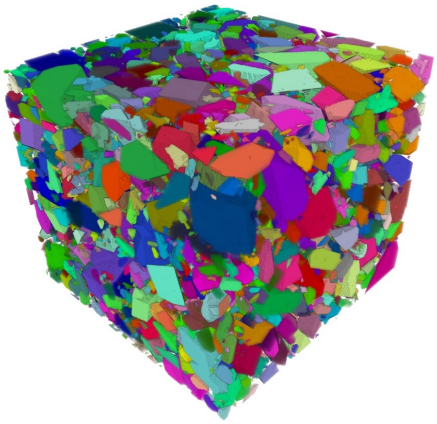

(d) segmented raw VI-RDX/Wax

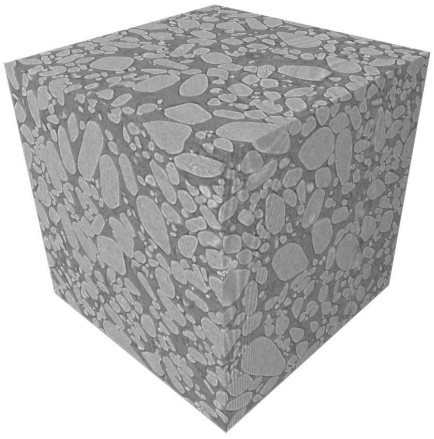

(e) μCT VI-RDX/Wax

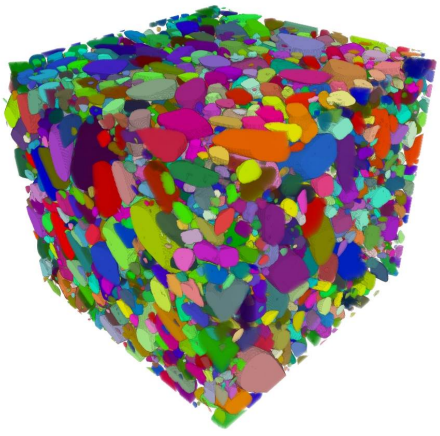

(f) segmented VI-RDX/Wax

Figure 3: Micro-computed tomography volumes and the corresponding segmentations

Table 1: Characteristics of the segmented volumes

	RS-RDX/Wax	raw VI-RDX/Wax	VI-RDX/Wax
Number of grains	12719	6080	7178
Number of extracted grains	11159	4751	5677
Volume fraction of RDX (%)	52.8	54.6	54.1

GENERATION OF VIRTUAL MICROSTRUCTURES

Virtual microstructures give us the possibility to work on ideal materials. For example, we are able to create a material with no intra-granular defects or three materials with different shape of particles but with the same size distribution. The idea is to uncorrelate some microstructural parameters to better understand their influence on the sustained shock sensitivity. These numerical materials are intended to be used in mesoscale finite element simulations to study the effects of the microstructure on the shock-wave propagation.

Virtual microstructures are particularly useful if they are representative of the real microstructures. Our virtual microstructures are built with the library of grains created from real material microstructures. The process used to construct the virtual microstructures guarantees their compliance with the real microstructures. The construction of the virtual model is based on the RSA (Random Sequential Adsorption) [17] principle. This principle is the following: a random grain is placed in a volume at a random position. If the grain intersects a previously placed grain, a new random position is selected until the grain 'fits' in the volume.

To begin with, we try to create one virtual microstructure representative of the segmented microstructure for the three materials. We need to verify if we are able to reach the volume fraction of 0.54 % and to respect the size distribution of RDX grains. 8 classes of grains are defined according to their volume to respect the size distribution. Then, we determine the percentage in volume of each class necessary to reproduced the μCT segmented volume distribution (after the Miles-Lantuéjoul correction).

The numerical materials generated are periodic in order to have 'cropped' grains on the border of the volume. The grains from each class are placed sequentially, from highest to lowest volumes. We place the first 20 grains at a random position and, in case of intersection, at a new random position. For the other grains, we move the grain in a previously determined direction in case of intersection. When the number of displacement exceeds the size of the volume (i.e. all the positions were tested along one direction), a new random position is selected. If after 50 attempts, the grains still does not 'fit' in the volume, we select a new grain. This process is repeated until the correct volume fraction of each class is reached and, finally, until the 0.54 volume fraction is reached.

Slices extracted from the μCT segmented volume and the numerically generated volume of VI-RDX/Wax are presented on Figure 4. Visually, the two microstructures seem similar.

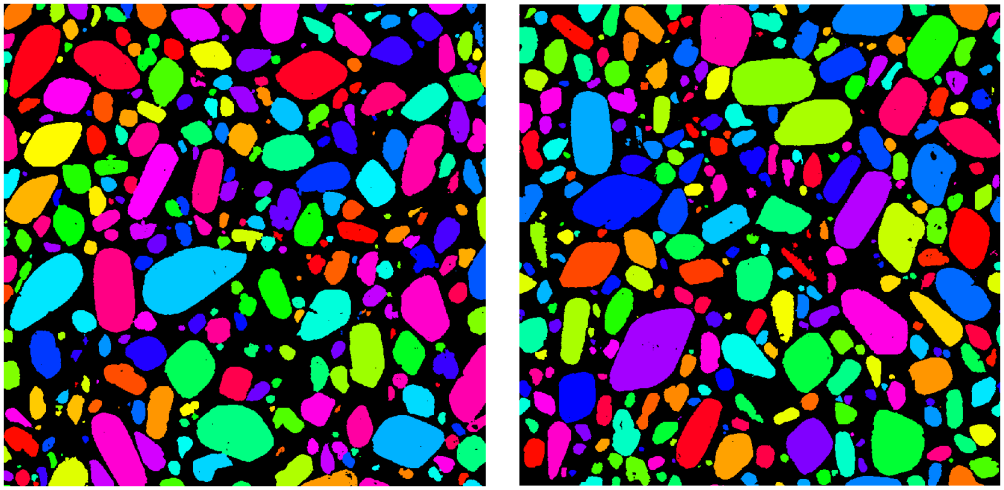

(a) segmented (b) virtual

Figure 4: 1000×1000 voxels sections from segmented and virtual models of the VI-RDX/Wax material

VALIDATION OF THE MICROSTRUCTURES

The μCT segmented microstructure and the virtual microstructure presented at Figure 4 are visually identical. We need to use descriptors to ascertain this visual impression. We use two descriptors to compare both real and virtual microstructures: i) the morphological granulometry of the grains and the matrix and ii) the spatial covariance.

The segmented volumes are converted into binary images (RDX grains/wax binder) so that we can compute the granulometry of each phase (Fig. 5). The determination of the granulometric curve is obtained with the residues of successive morphological openings operations defined as:

$$F_n(X) = 1 - \frac{Mes(\gamma_n(X))}{Mes(\gamma_0(X))} \tag{1}$$

where $\gamma_n(X)$ is the opening of size n on the subset X [18] and $Mes(X)$ is the Lebesgue measure (here the volume).

The virtual microstructures were generated to respect the volume distribution. The good correlation between the granulometric curve of the virtual and μCT volumes (Fig. 5a) indicates that 8 classes are enough to reproduce the size distribution of the grains. The granulometry of the matrix quantify the distance between the grains. This parameter is not controlled by the software developed to generate virtual microstructures but we still have good results (Fig. 5b). This allows to conclude that the granulometries of the virtual microstructure correspond to that of the segmented result of the imaged sample.

The second verification is the spatial covariance [19]. The spatial covariance $C_X(h)$ is the probability that two points x and $x + h$ lies on the same phase (Eq. (2)). As a consequence, $C_X(0)$ corresponds to the volume fraction p of the phase X. The covariance reaches a plateau for h_∞ which is equal to p^2.

$$C_X(h) = \{x \in X, x + h \in X\} \tag{2}$$

First the covariance is computed in the three orthogonal directions for the virtual material (Fig. 6a). The first observation is that the covariance measures are nearly identical which is consistent with an hypothesis of isotropy. Then we compare the covariance of the virtual and μCT volumes along one direction (Fig. 6b). The linear correlation coefficient is 0.9960 This allows one to conclude that the covariance of the virtual volume respects the one of the segmented volume.

Thus, we consider that the virtual microstructure generated with real grains of VI-RDX extracted from the μCT images is representative of the real microstructure.

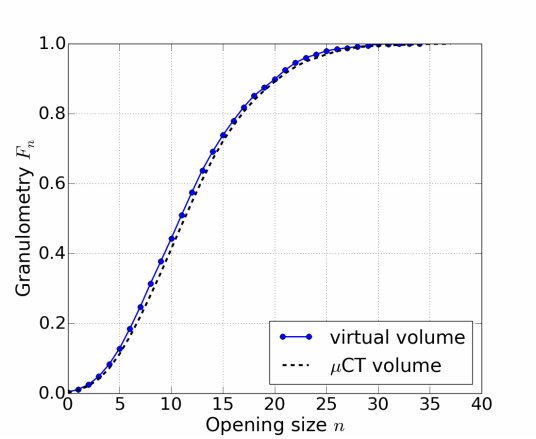

(a) RDX grains

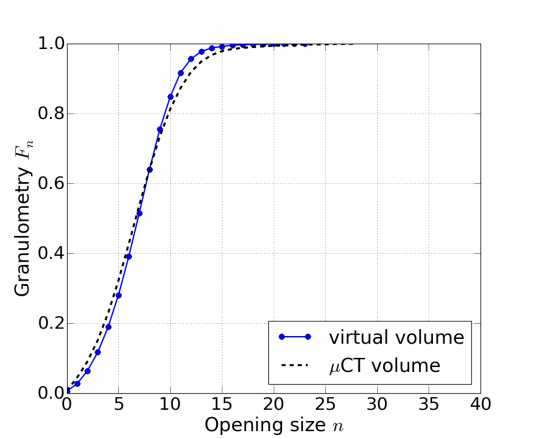

(b) Wax binder

Figure 5: Granulometry of (a) the grains and (b) the binder of the μCT segmented volume and of virtual volume for the VI-RDX/Wax material

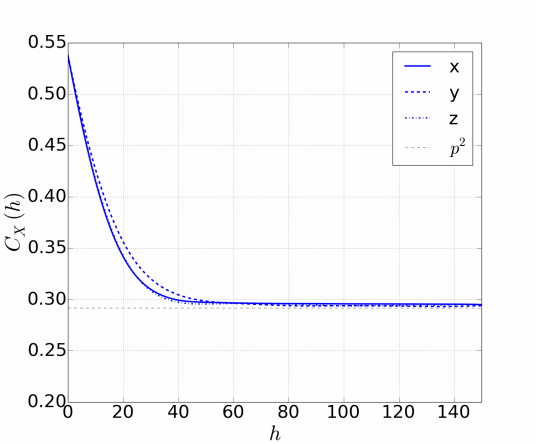

(a) Spatial covariance along ortogonal directions for the virtual VI-RDX/Wax material

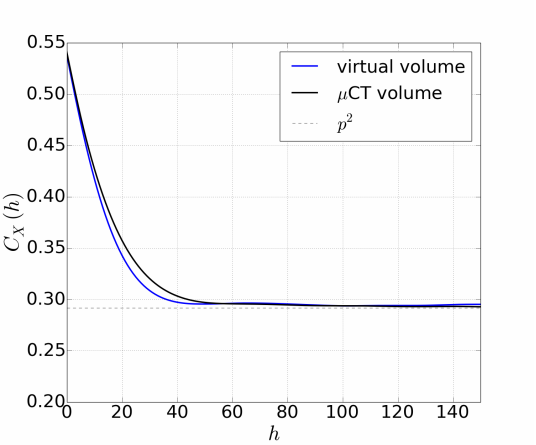

(b) Comparaison of the spatial covariances of the virtual and segmented volumes

Figure 6: Spatial covariance of the VI-RDX/Wax material

CONCLUSION

Three energetic materials composed of RDX/Wax (70/30 in weight) with different microstructures were imaged with micro-computed tomography. One large volume of each material (1000^3 voxels) is successfully segmented with the tool SAMG. The grains are extracted from these segmented volumes to create a library of grains. The library of grains is used to create virtual microstructures with the RSA method. We manage to reach the observed RDX volume fraction of the segmented μCT images of the real material and to respect the size distribution of grains. To verify that virtual microstructures are consistent with the μCT segmented volumes, we compare their binder and grains morphological granulometries and their spatial covariances. These two indicators allow us to validate the numerical materials.

FUTURE WORK

Three other independent 1000^3 voxels volumes are currently being segmented for each material. They will be soon exploited to increase the number of extracted grains and improve the statistical representativeness of the study.

The work presented in this paper aimed at creating virtual microstructures representative of μCT imaged real microstructures. This has been achieved by developing a microstructure generation software based on the RSA method. The next step is the generation of more controlled virtual microstructure by picking only the grains we are interested in (for instance only the spherical, without intra-granular defects ...). The objective is to reduce the correlations between microstructural parameters. These numerical materials will be used in mesoscale finite element simulations to study the effects of the microstructure on the shockwave propagation.

ACKNOWLEDGEMENTS

This work was partly supported by the French General Directorate for Armament (DGA) of the Ministry of the Armed Forces. The authors are also grateful to P. Rey (CEA Gramat) for its technical contribution to this project.

References

[1] F. P. Bowden and A. D. Yoffe. *Initiation and growth of explosion in liquids and solids.* Cambridge University Press, 1952.

[2] R. Menikoff. Pore collapse and hot spots in HMX. In *AIP Conference Proceedings*, volume 706, pages 393–396, 2004.

[3] R. Menikoff. Hot spot formation from shock reflections. *Shock Waves*, 21(2):141–148, April 2011.

[4] A. Barua. *Mesoscale Computational Prediction and Quantification of Thermomechanical Ignition Behavior of Polymer-Bonded Explosives (PBXs).* PhD thesis, Georgia Institute of Technology, August 2013.

[5] H. Moulard, A. Delclos, and J. W. Kury. The Effects of RDX Particle Size on the Shock Sensitivity of Cast PBX Formulations. In *Eight Symposium (International) on Detonation*, 1985.

[6] L. Borne. Influence of intragranular cavities of RDX particles batches on the sensitivity of cast wax bonded explosives. In *Tenth Symposium (International) on Detonation*, pages 286–293, 1993.

[7] L. Baillou, J.M. Dartyge, C. Spyckerelle, and J. Mala. Influence of crystal defects on sensitivity of explosives. In *Tenth Symposium (International) on Detonation*, pages 816–823, 1993.

[8] L. Borne. Explosive crystal microstructure and shock-sensitivity of cast formulations. In *Eleventh Symposium (International) on Detonation*, 1998.

[9] A. W. Campbell, W. C. Davis, J. B. Ramsay, and J. R. Travis. Shock initiation of solid explosives. *The Physics of Fluids*, 4(4):511–521, 1961.

[10] T. Chabardès. *Segmentation Automatique de Matériaux Granulaires.* PhD thesis, Mines Paristech, Fontainebleau, May 2018.

[11] Q. Yang. Recursive Bilateral Filtering. In *Computer Vision – ECCV 2012*, Lecture Notes in Computer Science, pages 399–413. Springer, Berlin, Heidelberg, October 2012.

[12] S. Beucher. Watershed, Hierarchical Segmentation and Waterfall Algorithm. In M. A. Viergever, J. Serra, and P. Soille, editors, *Mathematical Morphology and Its Applications to Image Processing*, volume 2, pages 69–76. Springer Netherlands, Dordrecht, 1994.

[13] T. Chabardès, P. Dokládal, M. Faessel, and M. Bilodeau. An affinity score for grains merging and touching grains separation. In *13th International Symposium on Mathematical Morphology*, volume 10225, pages 423–434, Fontainebleau, France, May 2017.

[14] R. E. Miles. On The Elimination of Edges Effects in Planar Sampling. In *Harding EF, Kendall DG*, pages 228–247, New York, 1974. Stochastic Geometry.

[15] C. Lantuejoul. On the estimation of mean values in individual of particles. *Microscopica Acta*, 5(266):73, 1980.

[16] L. Borne and J.-L. Patedoye. Device for measuring the density of particles by flotation, June 2009. US 7,607,341 B2.

[17] J. Feder. Random sequential adsorption. *Journal of Theoretical Biology*, 87(2):237 – 254, 1980.

[18] J. Serra. *Image Analysis and Mathematical Morphology.* Academic Press, Inc., Orlando, FL, USA, 1982.

[19] G. Matheron. *Random Sets and Integral Geometry.* Wiley, 1974.